Atomic Resolution Microscopy at the Solid-Liquid Interface

S.M. Lindsay, Ph.D.
Department of Physics
and Astronomy
Arizona State University
Tempe, AZ 85287-1504

and

Molecular Imaging Corp.
9830A S. 51st St.
Suite 124
Phoenix, AZ 85044

E-mail:
stuart.lindsay@asu.edu

Scanning tunneling and atomic force microscopes permit atomic-scale imaging of processes at the liquid-solid interface. This article reviews the mechanism of these microscopes. It also surveys some representative applications, such as the potential dependence of adlayer structure and the electron transfer properties of individual molecules.

The atomic structure of the liquid-solid interface has been, until now, a matter for modeling and the imagination of the analytical scientist. The invention of scanning probe microscopes—the scanning tunneling microscope and atomic force microscope—has opened this world to experimental examination. The microscopes operate on the simplest of physical principles—measuring the current or force between a pair of atoms as a means of profiling surfaces at atomic resolution—yet they let us invade complex territory. This review discusses the application of these simple methods in the complicated environment of the liquid-solid interface. Principles reviewed here include some examples of novel applications at the solid-liquid interface. The interested reader is referred to Chen (1) for illustrations of the basic techniques.

The solid-liquid interface, so vital to fields as diverse as electrochemistry, biology, and analytical chemistry, is now accessible to atomic-scale analysis, and we can look forward to developments as dramatic as those that ultrahigh vacuum technology brought to vacuum surface science.

Overview of the STM and AFM

The scanning tunneling microscope (STM) was invented by Binnig and Röhrer in 1981 (2,3) and the atomic force microscope (AFM) by Binnig and Quate in 1986 (4). Both the STM and the AFM work by placing a sensing probe within an atomic diameter or so of the surface to be probed. They rely on ingenious lever mechanisms which allow the probe tip to be moved very close to the surface with a mechanical drive. The remainder of the approach is made with a piezoelectric actuator (usually fabricated from lead zirconate titanate, or PZT). These change dimensions when a potential is applied to them, providing smooth displacements on the order of 1Å per volt. Similar materials are used to raster-scan the tip over the surface once adequate tunnel current (or interaction force) is obtained. In one mode (*constant current* or *constant force*), the sample or tip is moved up and down under computer control so as to maintain the current or force at a constant level as the tip is scanned over the surface. A typical image consists of a few hundred scan lines, each of which may be stored as a few hundred pixels in a computer. Each line is acquired in times that range from tens of milliseconds to a few seconds. Thus, whole images are obtained in times that range from several minutes to a few seconds. The displacement, as a function of position on the surface (x,y), is mapped onto a display to provide a quasi-three-dimensional rendering of the surface topography.

In the STM a metal tip is moved very close to a metal surface. A small voltage (millivolts to volts), applied between the two metals, drives a net flow of electrons as they tunnel between tip and substrate. This flow becomes measurable (picoamps to nanoamps)

when the distance between the tip and substrate is on the order of an atomic diameter. Tunneling by a particle has no classical analog, but it is familiar in the guise of the electron "sharing" that leads to chemical bonds. The STM is limited to the study of systems that are electronic conductors. It should be stressed at the outset that STM images are based on the electronic properties of a surface, and interpretation can be difficult (or impossible). However, high resolution is easily obtained, and the technique is simple. For these reasons, it is the technique of choice in electrochemistry where the substrate is, of necessity, an electronic conductor.

The AFM is used to study insulating surfaces. It works by measuring the deflection of a soft force-sensing cantilever as a probing tip is scanned over a surface. The quantum-mechanical "springs" that hold atoms together are about as stiff as mechanical springs that can be made in the lab (on the order of 0.1N/m spring constant). Therefore, a probe held by such a spring can be dragged over the surface of a solid without substantial damage. Soft springs are susceptible to vibrations, but the problem is alleviated by making them very light so that their resonant frequency is high. These are fabricated using integrated circuit manufacturing technology. A small pyrimidal protrusion at the end of a flexible cantilever contacts the surface. Minute deflections of springs may be sensed by an optical sensor. Vertical deflections of the cantilever are converted to angular deflections of a laser beam reflected from the end of the cantilever. The angular sensitivity is limited only by the laser power and noise in the system. It is relatively easy to sense sub-Ångstrom motion of the cantilever. The tip is lowered onto the surface until a deflection is detected. The sample is then scanned under the tip while a computer maintains a constant deflection signal. The required vertical deflection is mapped onto a display using electronics that are essentially identical to those in a STM controller. The set point deflection corresponds to forces (attractive or repulsive) of piconewtons (pN) to tens of nanonewtons (nN).

The atomic force microscope senses bonding between atoms at the end of a tip on a force-sensing probe and the atoms in the substrate. The strength of the bonds falls or rises with the amount of electron tunneling, so the AFM also has remarkble sensitivity and resembles STM in more than just the instrumentation. One important difference between the techniques lies with the fact that all the electrons in an atom can play a role in interaction forces, but only conduction (or *itinerant*) electrons carry currents.

The STM and AFM both use macroscopic probes, but the short range of interatomic interactions leads to a contrast that is dominated by the very end of the sensing probe. We illustrate this with the argument that first led Binnig to realize the extraordinary power of the STM (1). Tunnel current falls off with distance as

$$I \propto e^{-2\kappa z} \qquad \textbf{EQ1}$$

where 2κ is on the order of 1Å^{-1}. Therefore, a parabolic tip of radius R will have a lateral current distribution given by

$$I \propto \exp\{-2\kappa \frac{x^2}{2R}\} \qquad \textbf{EQ2}$$

With R = 1000Å, most (90%) of the current comes from a region of less than 100Å diameter, so high resolution is achieved with a blunt tip. Indeed, if the tip is not smooth but has a single atom asperity, then the current will come predominantly from the single atom at the end of the tip and atomic resolution becomes possible.

Electron tunneling in condensed matter is well studied (5), but the experimental demonstration that it could be exploited for atomic resolution at the liquid-solid interface was startling (6). The new field initiated through that work is the subject of this review.

The Controlled Liquid-Solid Interface

Atomic resolution microscopy under liquids has exciting new applications. Imaging surfaces (and processes) in their "real" environment is important for problems in chemistry, biology, and engineering. What is, perhaps, not so widely appreciated are the opportunities for advances in basic science.

Some of the complexity of a "real" interface is illustrated in the review by Stuve (7), who has used models of the liquid-solid interface in an ultrahigh vacuum environment to study the atomic structure by thermodynamic means and atomic scale probes like LEED. The first bilayer of water molecules on a close-packed metal surface is probably quite ordered, even if water does not react with the metal (i.e., does not chemisorb), and the metal surface is uncharged. The oxygen atoms orient toward the metal, and the second layer forms a network of hydrogen bonds with the first. If the surface is charged by, for example, applying a potential difference between it and another electrode in the same electrolyte, the ratio of anions to cations at the electrode surface will change to balance the electrode surface charge. The region of space over which a net charge is induced in the solution is referred to as the *double layer.* Most of the potential is dropped at the metal surface and where atoms and molecules are bound. A small fraction (ca. 25 mV) is dropped in a diffuse layer where molecules and ions undergo thermal motion.

This interface is remarkably complicated when compared with a clean surface in vacuum. However, this complication is compensated, to some extent, by two advantages of electrochemical interfaces. One is fundamental and lies in the possibility of *potential control* of the

F1

A microscope for electrochemical/in situ imaging at high resolution. The open liquid cell sits on a stainless steel plate (1) mounted to the microscope via adjustable screws (2), the height of which is controlled by a motor in the top-housing (3). A scanner housing (4) holds either a scanning tunneling probe or an atomic force sensing probe moved inside the sample chamber (5) through a flexible hermetic seal. Hermetic enclosure of the sample chamber permits control of the humidity or sparging with inert gasses for enhanced range of potential control of the sample.

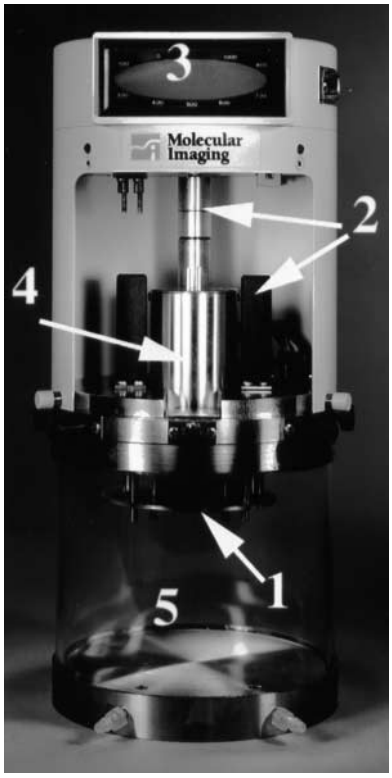

electrode. The second is practical —the relative ease with which contamination may be controlled.

Adsorption and the electric potential difference between the electrode and the bulk solution (i.e., outside the double layer region) are intimately connected. When a particle adsorbs onto a surface, some charge is redistributed between the surface and particle. This change in charge distribution leads to a change in the electric potential of the surface (i.e., electrode) onto which the particles adsorb. Conversely, by controlling the potential of the electrode with respect to the source of particles (the bulk fluid), adsorption may be controlled. The Gibbs-Duhem equation is a quantitative statement of this relationship. The change in energy per unit area of a rigid surface of charge density σ on adsorption of a surface excess (excess with respect to the bulk concentrations) Γ_i of species i is

$$d\gamma = -\sigma d\phi - \sum_i \Gamma_i d\mu_i \qquad \textbf{EQ3}$$

where $d\phi$ is the change in potential of the surface with respect to the reservoir of particles and $d\mu_i$ is the change of chemical potential of species i on binding to the solid. In a UHV experiment, the adsorption (Γ_i) is controlled by isolating the surface from the reservoir of particles. The system is kept far from equilibrium and the potential of the surface with respect to the source of particles is not controlled. In an electrochemistry experiment, the (conducting) surface is in contact with the source of particles, and adsorption is controlled using a feedback system to fix the surface potential. Thus, the UHV and electrochemical environments are complementary ways of preparing *controlled surfaces.*

The second advantage is a practical one. The techniques outlined above only permit control to the extent that a reactive species (large $d\mu_i$) does not cover the surface. If a solid layer of the reaction product is in equilibrium with the dissolved (reactive) ions, attempts to alter the surface charge (or potential, $d\phi$) change only the relative amount of reactants and products, leaving the surface pinned at the Nernst potential for the reaction. Thus, the concentration of reactive atoms or molecules must be kept small. At first sight, the situation appears to be hopeless. To use a concrete example, chlorine ions can react with gold, so electrolytes such as NaCl do not permit a large variation of the interfacial potential at a gold electrode. Perchlorate electrolytes do not interact strongly with gold, but it is difficult to prepare perchlorate solutions with less than 10^{14} chlorine ions per cm^3. This concentration of contamination in a vacuum chamber would be disasterous. The corresponding partial pressure of 10^{-3} Torr would form a monolayer in just one millisecond. However, in a liquid, ions move more slowly, covering a distance l cm in a time $t \approx l^2/D$ seconds where D is the translational diffusion constant. In the example just discussed, about 10^{14} ions/cm^2 would form a monolayer, so diffusion would have to transport ions over a distance of $\approx$ 1 cm. With a typical value for D of around 10^{-6} cm^2s^{-1} this would take 10^6 seconds (more than a week)! To achieve such results in a UHV experiment would require a pressure of 10^{-12} Torr, an excellent vacuum.

Atomic Resolution Microscopy in Water

The practical extension of STM techniques to operation in water was straightforward. The current that flows when ions react with an electrode is proportional to the electrode area, whereas tunneling requires only that a single exposed metal atom be available at the end of the tip. Liu, et al. (8) and Sonnenfeld and Hansma (6) showed that electrochemical leakage current into the surrounding electrolyte could be minimized by coating the tip with an insulating layer, leaving only the very end open to act as a source (or sink) of tunnel current. Using glass-coated microelectrodes, Sonnenfeld and Hansma obtained atomic resolution images of graphite under water and images of a polycrystalline gold surface in a salt solution (6). Their microscope was very simple. A tunneling tip was suspended from piezoelectric scanning tubes and hung into a liquid container placed over a graphite substrate. The sample was mounted on a steel plate that was bent up towards the tip until tunneling current was obtained.

An example of a modern microscope for fluid studies is shown in ***F1***. The tip of an AFM or STM dips down into the liquid cell which consists of a small Teflon tube mounted on a steel sample stage (***F1.1***). The stage is positioned vertically with screws (***F1.2***) and a stepper motor inside the top housing (***F1.3***). A scanner unit (***F1.4***) moves an STM or AFM probe through a flexible hermetic seal. The whole sample stage is hermetically isolated in a glass container (***F1.5***). This microscope is capable

F2

Gold (111) surface showing stripes owing to the 23 x √3 reconstruction. This structure is lifted at positive potentials, and the STM has been used to study the kinetics of this transition.

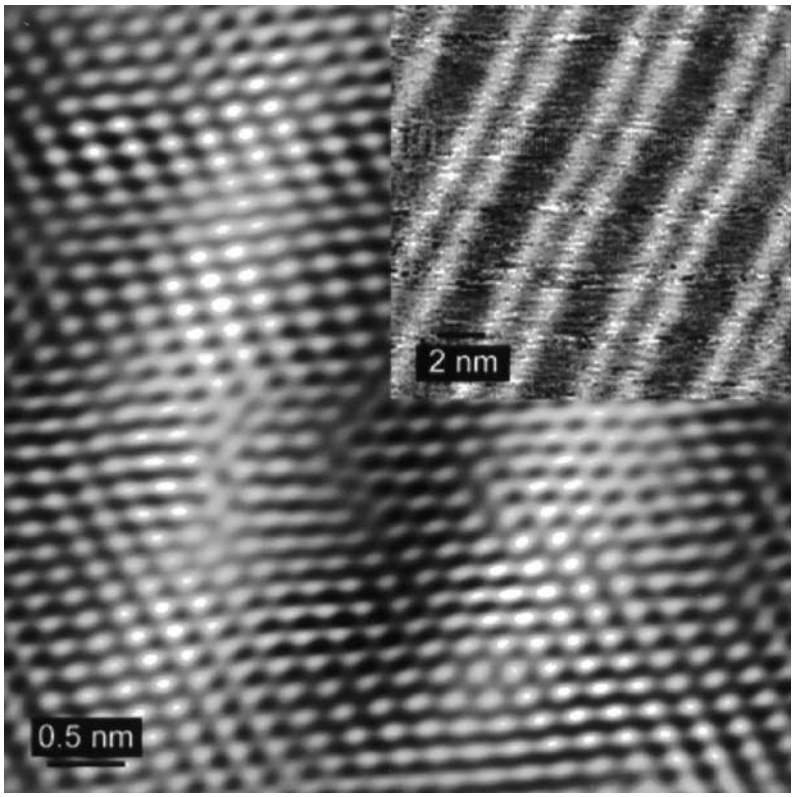

F3

Two sequential scans of a cytosine adlayer taken just after the potential was stepped into the region where it disorders. Melting of the ordered layer is seen to proceed along rows of molecules.

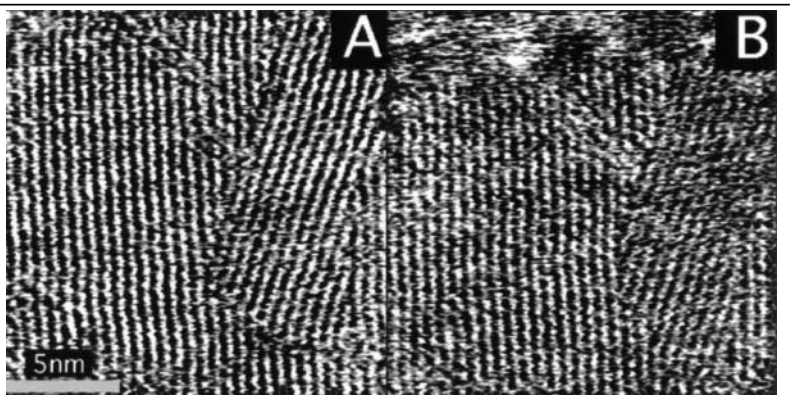

of drifting as little as 1Å/minute, operating in water.

Though the experimental arrangements are simple, we must address the complexities of the medium. There is, presumably, a cluster of molecules between the scanning probe and the substrate. How does this cluster influence the interaction force and the tunnel current? We shall return to this point.

Applications of STM and AFM Imaging

Before considering the physical principles of the operation of the microscopes, we will survey some applications representative of growing areas of the field. This is not intended to be a comprehensive review. Electrochemical applications have been surveyed elsewhere (9,10 and Volume 94 of *Discussions of the Faraday Society*, which is devoted to "The Liquid-Solid Interface at High Resolution").

We begin with a rather special example of the operation of an AFM in water. Operation in water has yet an additional advantage for atomic force microscopy. The principal limitation in air is capillary condensation of water into the gap between the tip and the substrate, which leads to a large adhesive force which pulls the tip into the surface. By imaging a low-energy surface (i.e., intrinsically low adhesion) under water, Ohnesorge and Binnig were able to lower an AFM tip into contact gently, sensing the changes that occurred as the atoms first pulled the tip in via attractive interactions (11). As the tip was brought closer to the surface, the contrast started to change, becoming negative as repulsive forces contributed to the interaction. Eventually more than one tip atom became involved, complicating the image. Importantly, there was *no* evidence of image contrast from water molecules bound to the substrate, implying that, on this low energy (calcite) surface, interactions with water molecules are very weak.

Rather delicate surface structures can be imaged. ***F2*** is an image of the fine structure formed when the gold (111) surface reconstructs. Reconstruction is driven by a lowering of the surface energy obtained by redistributing the surface curvature. Describing this requires relaxing the constraint that the surface is rigid in ***EQ3***. In the case of gold, a few extra gold atoms move to the surface to cause a small buckling. The small (0.1Å high) ripples caused by these stacking faults are seen as stripes in the image. The images were obtained by STM with the sample under potential control in 0.1M $HClO_4$ (12-14).

Changes of the surface potential can be used to put down (and remove) adlayers in a controlled manner. An example is the deposition of Cu on Au(111) imaged by STM (15) where the hexagonal Cu lattice that covers the gold terraces has nearly twice the lattice constant of the underlying gold. This process has also been imaged by AFM (16).

The deposition process is illustrated dramatically by potential-jump (or potentiodynamic) experiments. In these experiments, the surface potential is jumped into the adsorption region as the microscope is scanning and the surface is seen

F4

AFM images showing corrosion of 304 stainless steel in NaCl solution. Images were taken after 4 minutes (A – height range = 50 nm), 30 minutes (B – height range = 250 nm) and 150 minutes (C – height range = 500 nm).

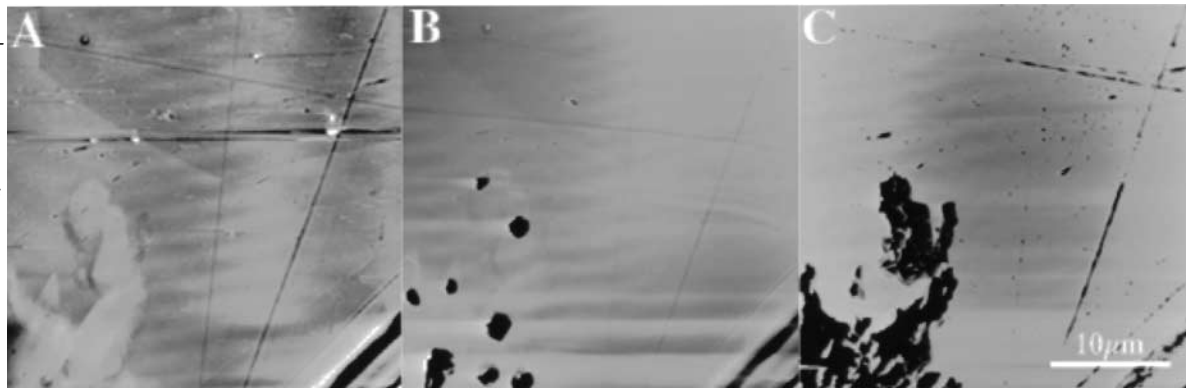

F5

AFM scans of zinc foil in aqueous electrolyte (A) on first immersion and (B) after two potential cycles.

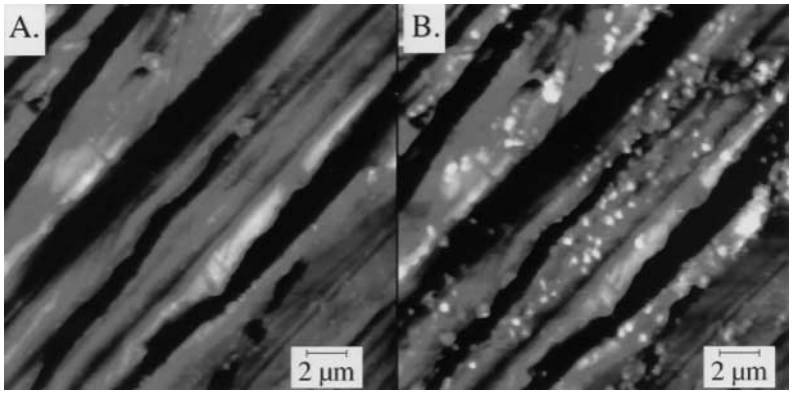

to change structure instantaneously on the time-scale of the scan. Gao, et al. have made dramatic images of adsorption of iodine onto gold (17).

Much progress has been made in studying the deposition of organic molecules. ***F3*** shows ordered stacks of cytosine molecules on Au(111). At positive potentials, cytosine chemisorbs on gold, forming a highly ordered adlayer. The images show the progression of melting of the ordered regions as the potential is stepped just negative of the chemisorption region (18). The adlayer is present in the "melted" regions, but is, presumably, diffusing too rapidly to yield images. In the case of bipyridine on Au(111), adsorption in the disordered phase is strong enough to inhibit diffusion, and individual molecules can be followed from the ordered to disordered phase (19).

Applications of AFM to Biological Processes

Microscopy in water offers the possibility of imaging processes as they occur, and perhaps the first example of this type of experiment was the imaging of thrombin-promoted aggregation of fibrinogen. The AFM was used to image a clean glass slide under a solution of the blood-clotting protein fibrinogen. The clotting enzyme thrombin was added at the beginning of a series of scans and subsequent scans showed the formation of aggregated mats of fibrinogen (20).

In addition to imaging, the AFM can make local force measurements. Li, et al. measured the electrostatic interaction between small charged polystyrene latex spheres by gluing one sphere onto a force-sensing cantilever and scanning it over a sphere attached to a mica substrate (21). A long-range repulsive interaction was seen in a low-salt medium. It became screened as the salt concentration was increased. Hoh, et al. measured small jumps in the adhesive interaction between a silicon nitride tip and a glass surface in a basic solution (22). The force-interval between jumps shows a distinct periodicity. Each step in adhesive force was separated by about 10 pN, a force that the authors attribute to the breaking of a single hydrogen bond. Such experiments have become very sophisticated and the AFM has been used to measure the force required to separate complementary strands of DNA (23).

Other examples include the measurement of enzyme motions when acting on a substrate and the imaging of the formation of various DNA-protein complexes (24).

Large-Scale Electrochemical AFM Imaging

The STM has proven valuable in the study of electrode processes such as corrosion and the modification of battery electrodes under potential cycling where information on the morphology of electrodes is useful, even at low resolution. ***F4*** shows the action of sodium chloride on 304 stainless steel over a period of 150 minutes. ***F5*** shows the surface of a Zn battery electrode as freshly prepared (A) and after two potential cycles (B).

What Do STM Images in Water Mean?

A simple model of the vacuum tunneling gap (25) shows that the current decays according to ***EQ1*** with

$$\kappa = \sqrt{\frac{2m}{\hbar^2}\Phi} \qquad \textit{EQ4}$$

where the work function, Φ, is the work required to remove an electron from the bulk of the metal to a position, at rest, outside the metal.

F6

Images of a mixed film of protoporphyrin and iron-protoporphyrin on graphite under potential control with the substrate held at the redox potential of the iron. (A) No iron. (B) 20% iron. (C) 80% iron. (D) 100% iron.

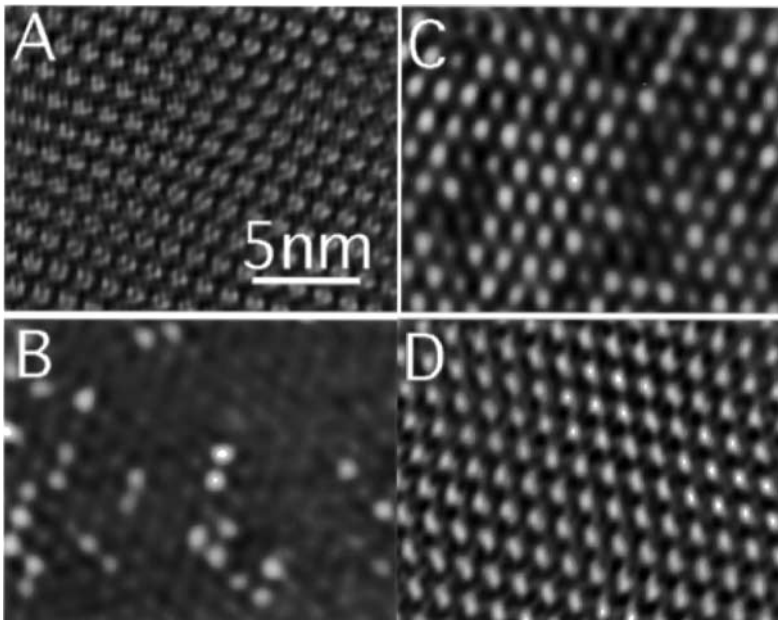

F7

Images of DNA microcircles on mica taken under 1mM $ZnCl_2$ solution showing kinks in the DNA which form only in the presence of zinc ions. The full width of the images is about 3 nm and internal structure is evident.

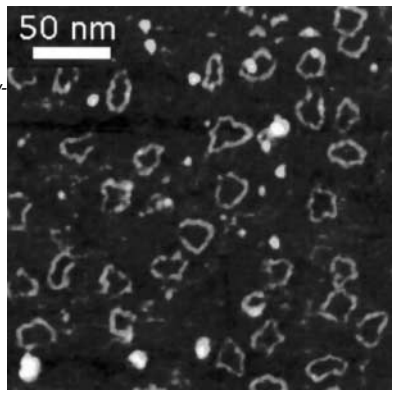

EQ1 and ***EQ4*** show that the tunnel current though the gap will fall as

$$\exp\{-1.025\sqrt{\Phi}\,z\}$$

when Φ is measured in eV and z is measured in Å. For work functions on the order of a few eV, the tunnel current will decay by about an order of magnitude for each Å change in gap (the origin of the extraordinary sensitivity of the STM).

How realistic is this simple picture of a metal-vacuum-metal gap? It is certainly not valid for tunneling in a medium. To see this, we need to consider how the resistance of a small tunnel junction changes with distance. At *contact*, the situation becomes particularly simple if the junction is small enough.

The resistance of classical point contacts is described in terms of the bulk resistivity of the materials that form the contact. The "constriction resistance" is a simple function of the resistivity of the materials. For a contact of diameter a, the constriction resistance is given by $R \approx \rho/a$ where ρ is the resistivity of the metal (26). This is not a relevant description when the dimensions of the contact become smaller than the mean-free path of electrons in the materials used to make the contact. Such electrical systems are often referred to as *mesoscopic* (27). This difference was first pointed out by Sharvin in 1965 (28). He used classical arguments to estimate the resistance of a gas of electrons diffusing through a small orifice. Landauer has considered the contribution of a single scattering point to the total resistance of a linear (but disordered) array of scatterers (29). The result, *independent of the material of the constriction*, is

$$R_0 = \frac{h}{2e^2} = 12.9\kappa\Omega \qquad \textbf{EQ5}$$

The wavelength of electrons at the Fermi energy is somewhat longer than typical atomic dimensions (30), so a single atom point-contact will act like a one-dimensional constriction. Further examination shows that this result is remarkably robust. It is (more or less) true in three dimensions, even for adsorbed atoms with states that are far from resonance. Lang has carried out simulations of the quantum point-contact resistance of an STM (31) and Kalmeyer and Laughlin have derived some useful formulae for the quantum point contact resistance of an atom (32). The resistance of these contacts is on the order of $10^4\Omega$ for a remarkable range of parameters.

Thus, we conclude that the resistance of a vacuum tunnel junction should vary with distance according to

$$R(z)=12.9e^{2\kappa z}k\Omega \qquad \textbf{EQ6}$$

We have made careful measurements of the tunneling gap in water (33) concluding that, at $R \approx 10^9\Omega$, the gap is about 20Å. According to ***EQ6***, this gap in vacuum would correspond to $10^{24}\Omega$ tunneling resistance!

Of course, a gap containing molecules must differ from a vacuum gap. A simple model of molecules in a gap is based on a one-dimensional model of *resonant* tunneling. Even far from resonance (i.e., the electron energies are not close to energies of molecular states), the molecular states may enhance tunneling considerably (34-36). Nonetheless, there is currently no good understanding of the extreme range of tunneling in water, although many electron effects (polarization) probably play a role (37). Certainly, it is remarkable that atomic resolution is obtained when the tip is far from the surface. While the water between the tip and substrate may be invisible in the image, it plays an important role in the tunneling process.

STM Measurement of Molecular-Electronic Properties

Given the theoretical uncertainties discussed above, it would seem that, in spite of the plethora of evocative images, the STM should be avoided at all costs, for what good is high resolution if we cannot

interpret it? Indeed, recent advances in AFM have led to considerable enhancement of its resolution in water (see below), so the original reasons for using STM are not as compelling.

However, the ability of the STM to probe local electronic properties is of considerable value. Recent work by Tao and others has shown that there is a significant correlation between STM contrast and the electrochemical properties of molecular adlayers (38-41). Thus, the STM has a role as a nanoscale analytical device, capable of chemical identification of individual molecules in certain cases.

F6 shows images of mixed films of protoporphyrin and iron protoporphyrin imaged on a graphite electrode held at the redox potential of the iron. The images show a film with no iron (***F6A***), 20% iron-containing molecules (***F6B***), 80% iron-containing molecules (***F6C***), and 100% iron-containing molecules (***F6D***). The bright spots, which light up when the substrate potential is set at the redox potential, correspond to the location of iron-containing porphyrins.

Improved AFM Imaging in Fluids

Conventional contact-mode AFM results in considerable damage to the surface, particularly when soft adlayers are imaged under water. An improvement results if the tip is oscillated so that the surface is contacted only intermittently, and a method (called fluid tapping) has been developed by several groups (42,43). The cantilever is vibrated by means of a piezoelectric actuator attached to the fluid-cell housing. Unfortunately, damping of the cantilever motion by water requires that the actuator be vibrated at large amplitudes, and this drive causes spurious mechanical resonances in the microscope housing (44). A significant improvement results if the tip is driven directly. One scheme for doing this is to apply a magnetic film to the cantilever and use a solenoid to generate a magnetic field at the cantilever (45,46). If the other components of the microscope are not magnetic, spurious responses are eliminated (47). Remarkable resolution of biological molecules under water has been obtained with this approach (48). An example is shown in ***F7***. This is an image of small (180Å diameter) synthetic DNA microcircles. Abrupt kinks form in the presence of Zn ions. They disappear in the presence of Mg ions (49).

Conclusions

It has been a little over ten years since the discovery that the STM can image atoms in water. Yet the field has undergone rapid growth only recently as special microscopes become available commercially. Further rapid development of instruments is inevitable, and we expect to see particularly rapid progress in the imaging of *processes* at the liquid solid interface and the development of molecular-electronic devices and processes based on single molecules.

Acknowledgments

This work was supported in part by grants from the NSF and Molecular Imaging Corporation. I am grateful to Nongjian Tao, David Lampner, David Uhl and James Hudson for supplying images.

References

1. *C.J. Chen in "Introduction to Scanning Tunneling Microscopy," Oxford University Press, New York, 1993.*
2. *G. Binnig, H. Röhrer, C. Gerber, and E. Weibel, Phys. Rev. Lett. 49 (1982) 57.*
3. *G. Binnig and H. Röhrer, Rev. Modern Phys. 59 (1987) 615.*
4. *G. Binnig, C.F. Quate, and C. Gerber, Physical Review Letters 56 (1986) 930.*
5. *C.B. Duke in "Tunneling in Solids . Solid State Physics" Vol. 10 (F. Seitz, D. Turnbull, and H. Ehrenreich, Eds.), Academic Press, New York, 1969, p. 353.*
6. *R. Sonnenfeld and P.K. Hansma, Science 232 (1986) 211.*
7. *E.M. Stuve and N. Kizhakevariam, J. Vac. Sci. Technol 11 (1993) 2217.*
8. *H.-Y. Liu, F.R.F. Fan, C.W. Lin, and A.J. Bard, J. Am. Chem. Soc. 108 (1986) 3838.*
9. *H. Seigenthaler in "STM in Electrochemistry, in Scanning Tunneling Microscopy II" (R. Wiesendanger and H.J. Güntherodt, Eds.) Springer-Verlag, Berlin, 1992, p. 7.*
10. *A. Bard and F.R.F. Fan in "Applications in Electrochemistry, in Scanning Tunneling Microscopy: Theory, Techniques and Applications" (D.A. Bonnell, Ed.), VCH, New York, 1993, p. 287.*
11. *F. Ohnesorge and G. Binnig, Science 260 (1993) 1451.*
12. *N.J. Tao and S.M. Lindsay, Surf. Sci. Letts. 274 (1992) L546.*
13. *O.M. Magnussen in "In-situ Rastertunnelmikroskop-Untersuchungen zu Rekonstruktion, Anionadsorption und Unterpotentialabscheidung auf Goldelektroden" Universität Ulm, 1993.*
14. *X. Gao, A. Hamelin, and M. Weaver, J. Chemical Physics 95 (1991) 6993.*
15. *O.M. Magnussen, J. Hotlos, G. Beitel, D.M. Kolb, and R.J. Behm, J. Vacuum Science and Technology B 9 (1991) 969.*
16. *S. Manne, P.K. Hansma, J. Massie, V.B. Elings, and A.A. Gewirth, Science 251 (1991) 183.*
17. *X. Gao and M.J. Weaver, J. Am. Chem. Soc. 114 (1992) 8544.*
18. *T. Wandlowski, D. Lampner, and S.M. Lindsay, J. Electroanal. Chem. 404 (1996) 215.*
19. *F. Cunha and N.J. Tao, Phys. Rev. Lett. 75 (1995) 2376.*
20. *B. Drake, C.B. Prater, A.L. Weisenhorn, S.A.C. Gould, T.R. Albrecht, C.F. Quate, D.S. Cannell, H.G. Hansma, and P.K. Hansma, Science 243 (1989) 1586.*
21. *Y.Q. Li, N.J. Tao, J. Pan, A.A. Garcia, and S.M. Lindsay, Langmuir 9 (1993) 637.*
22. *J.H. Hoh, J.P. Cleveland, C.B. Prater, J.-P. Revel, and P.K. Hansma, J. Am. Chem. Soc. 114 (1992) 4917.*
23. *G.U. Lee, L.A. Chrisey, and R.J. Colton, Science 266 (1994) 771.*
24. *H.G. Hansma, J. Vac. Sci. Technol. (1996).*
25. *R.L. Liboff in "Introductory Quantum Mechanics," Holden-Day Inc., Oakland, 1980.*
26. *F. Llewellen-Jones in "The Physics of Electrical Contacts," Oxford University Press, Oxford, 1957.*

27. *Y. Imry in "Physics of Mesoscopic Systems, in Directions in Condensed Matter Physics" (G. Grinstein and G. Mazenko, Eds.), World Scientific Publishing, Philadelphia, 1986, p. 101.*
28. *Y.V. Sharvin, Soviet Physics JETP 21 (1965) 655.*
29. *R. Landauer, Philosophical Magazine 21 (1970) 863.*
30. *N.W. Ashcroft and N.D. Mermin in "Solid State Physics," Holt, Rinehart and Winston, New York, 1976.*
31. *N.D. Lang, Phys. Rev. B 36 (1987) 8173.*
32. *V. Kalmeyer and R.B. Laughlin, Phys. Rev. B35 (1987) 9805.*
33. *A. Vaught, T.W. Jing, and S.M. Lindsay, Chemical Physics Letters 236 (1995) 306.*
34. *S.M. Lindsay, O.F. Sankey, Y. Li, and C. Herbst, J. Phys. Chem. 94 (1990) 4655.*
35. *P. Sautet and C. Joachim, Ultramicroscopy 42-44 (1992) 115.*
36. *C. Joachim and P. Sautet in "Electron Tunneling Through a Molecule, in Scanning Tunneling Microscopy and Related Methods" (R.J. Behm, Ed.), Kluwer, Netherlands, 1989, p. 377.*
37. *A. Mosyak, A. Nitzan, and R. Kosloff, J. Chem. Phys. (1996).*
38. *W. Han, E.N. Durantini, T.A. Moore, A.L. Moore, D. Gust, P. Rez, G. Leatherman, G.R. Seely, N. Tao, and S.M. Lindsay, J. Phys. Chem., submitted.*
39. *N. Tao, Physical Review Letters 76 (1996) 4066.*
40. *S.R. Snyder and H.S. White, J. Electronanal. Chem. 394 (1995) 177.*
41. *U. Mazur and K.W. Hipps, J. Phys.Chem. 99 (1995) 6684.*
42. *P.K. Hansma, J.P. Cleveland, M. Radmacher, D.A. Walters, P.E. Hilner, M. Bezanilla, M. Fritz, D. Vie, H.G. Hansma, C.B. Prater, J. Massie, L. Fukunaga, J. Gurley, and V. Eilings, Appl. Phys. Lett. 64 (1994) 1738.*
43. *C.A.J. Putman, K.O.V.d. Werf, B.G. deGrooth, N.F.V. Hulst, and J. Greve, Applied Physics Letters 64 (1994) 2454.*
44. *T.E. Schaffer, J.P. Cleveland, F. Ohnesorge, D.A. Walters, and P.K. Hansma, J. Applied Physics 80 (1996) 3622.*
45. *S.M. Lindsay, Y.L. Lyubchenko, N.J. Tao, Y.Q. Li, P.I. Oden, J.A. DeRose, and J. Pan, J. Vac. Sci. Technol. 11 (1993) 808.*
46. *S.J. O'Shea, M.E. Welland, and J.B. Pethica, Chemical Physics Letters 223 (1994) 336.*
47. *W. Han, S.M. Lindsay, and T. Jing, Applied Physics Letters 69 (1996) 4111.*
48. *W. Han, S.M. Lindsay, M. Dlakic, and R.E. Harrington, Nature 386 (1997) 563.*
49. *W. Han, M. Dlakic, R.E. Harrington, J. Zhu, and S.M. Lindsay, PNAS, in press.*